J Therm Anal Calorim (2011) 105:705–718
DOI 10.1007/s10973-011-1508-7

Thermophysical properties and material modelling of acrylic bone cements used in vertebroplasty

Sebastian Kolmeder · Alexander Lion · Ralf Landgraf · Jörn Ihlemann

ESTAC2010 Conference Special Issue

Abstract The stabilization of osteoporotic vertebrae with acrylic bone cement, called vertebroplasty, is a common procedure in modern surgery. However, the thermo-mechanical-chemically coupled material behaviour of curing bone cements makes the application even for experienced surgeons difficult and can lead to potential complications like heat necrosis, leaking bone cement, embolisms and postoperative load shifting. In order to reduce these potential complications, to minimize the risks and to better understand the occurring effects, the thermophysical properties of a commercial acrylic bone cement were investigated in detail using differential scanning calorimetry, volumetric dilatometry and temperature controlled rheometry. More specifically, the reaction kinetics, the specific heat, the thermal conductivity, the thermal expansion, the chemical shrinkage as well as the mechanical behaviour was studied during the reaction process of the bone cement. Furthermore, the explored material behaviour is described by a customized material model that takes into account all observed effects. With the aid of this model the inhomogeneous chemical, thermal and mechanical states that appear during the application and curing of acrylic bone cements, can be studied by finite element treatment.

Keywords Acrylic bone cement · Differential scanning calorimetry · Rheometry · Volumetric dilatometry

S. Kolmeder (✉) · A. Lion
Institute of Mechanics, Faculty of Aerospace Engineering, University of the Federal Armed Forces, Neubiberg, Germany
e-mail: sebastian.kolmeder@unibw.de

R. Landgraf · J. Ihlemann
Institute of Mechanics and Thermodynamics, Faculty of Mechanical Engineering, Chemnitz University of Technology, Chemnitz, Germany

Introduction

Acrylic bone cements are widely used to reinforce affected vertebrae that have come down with osteoporosis and even maybe fractured. A polymer powder and a monomer liquid are mixed together to form the actual bone cement, which has initially the consistency of a dough. This dough is filled into a syringe and connected to a biopsy needle by a flexible tube. Preliminary to the mixing, the biopsy needle is inserted into the affected vertebra via the patient's back and the pedicle of the vertebral arch. Owing to a swelling process and the starting radical polymerisation the viscosity of the cement rises. Having the right consistency the cement is injected into the vertebra, penetrates it and fills out the cavities. An X-ray apparatus enables the surgeon to monitor the radio-opaque cement-flow inside the vertebral body. The bone cement hardens throughout the proceeding exothermal polymerisation process and stabilizes the treated vertebra within the spinal column. Chemical shrinkage, thermal expansion as well as an increase of the viscosity and stiffness accompanies the polymerisation reaction. The coupling of these effects complicate a correct and effective operation procedure. Potential side effects are, among others, heat necrosis caused by excessive heat generation, a leakage of bone cement into surrounding tissue and the risk of embolisms due to toxic monomer. Moreover, the treated vertebra provokes a load shift within the spinal column. That means that adjacent vertebrae are exposed to major and different loadings, because of the increased stiffness of the bone-cement-filled vertebra. It is likely that this load shifting leads to further fractures in these vertebral bodies. In order to get a clear understanding of the processes going on during a vertebroplastic procedure as well as to minimize the risks of a failed surgery and to avoid postoperative complications, a finite element analysis of the surgery

process can provide valuable information. For this purpose several models were developed in literature, that describe the thermochemical and thermomechanical behaviour of bone cements. Mazzullo et al. [1] present a thermochemical model for polymerizing acrylic cements, that accounts for uncomplete curing. Maffezzoli et al. [2] also consider the induction time, the time between mixing the two cement ingredients and the onset of polymerisation, in their kinetic model. In a further article Lingois et al. [3] expand a thermochemical model, similar to the kinetic models mentioned above, by an isothermal viscoelastic mechanical approach. Furthermore, this model is able to predict chemical shrinkage. Similar approaches are given by Briscoe and New [4] and Perez et al. [5]. Both couple the mechanical behaviour of bone cement to the thermochemical properties. A completely different aspect of modelling is focused by Beaudoin [6] and others [7–11]. The viscous flow of cements, used in vertebroplasty, is simulated by means of a power law, that describes the rising viscosity with proceeding time. Meng [12] presents in his work a technique for the patient-specific simulation of a vertebroplastic procedure. Besides the bone modelling based on CT-Data, the same power law is applied for the mechanical properties of the cement in [12]. However, thermal properties are neglected in this work. There are several studies, that deal with the postoperative behaviour of acrylic bone cements. In contrast to Baroud et al. [13] and Rohlmann et al. [14], which perform their computations on a pure elastic constitutive law, Lion et al. [15] present a viscoelastic approach to describe the frequency dependent material behaviour of bone cement.

In the this article, a material model is introduced, that is able to represent the thermomechanical-chemically coupled material behaviour of acrylic bone cement in-depth. Especially the temperature- and cure-dependent thermal properties as well as the thermoviscoelastic behaviour are included. Based on a model for curing adhesives, originally developed by Lion and Höfer [16], minor modifications were made to adopt it for the bone cement material. A detailed experimental database of the bone cement, including the reaction kinetics, the specific heat and released heat, the chemical shrinkage and the thermal expansion as well as the mechanical behaviour, was the foundation for parametrising the model.

Material

As mentioned above, acrylic bone cements are mixed of two components, a polymer powder and a liquid monomer. The powder consists of spherical Polymethylmethacrylate (PMMA) and co-polymerised Methylmethacrylate (MMA) with a typical particle size of 50 μm. To trigger the radical polymerisation, the powder contains dibenzoyl peroxide (BPO) as an initiator and the liquid contains dimethyl-para-toluidine (DMpT) as an activator, that form free radicals when getting in contact with each other. For X-ray visibility zirconium dioxide is added to the powder as well as antibiotics and a dye for colouring. The liquid is mainly composed of Methylmethacrylate. Other ingredients are the activator DMpT, also a dye and small amounts of hydroquinone to avoid polymerisation of the liquid while stored.

When both components get in contact with each other, a dissolution process starts. The initiator BPO and the activator DMpT form free radicals, that are tied by the inhibitor hydroquinone first. After the complete amount of hydroquinone is consumed, MMA molecules start to adsorb to free radicals and build up polymer chains. The chain growth stops whenever two growing ends of chains meet. Osteopal V, a common bone cement applied in vertebroplasty and manufactured by Heraeus Medical, Germany, has been examined and characterised in this study.

Experimental characterisation

Reaction kinetics

The thermophysical material properties of curing bone cement depend primarily on the degree of cure i.e., on the progress of the polymerisation, and on temperature. Therefore, it is reasonable to investigate the curing reaction at first. This was done by differential scanning calorimetry (DSC), using sample weights from 5–8 mg in pierced aluminium pans. A general view on the physical processes taking place in a DSC-apparatus is given in [17]. Isothermal curing experiments of 1 h duration were performed on a DSC 204 F1 Phoenix, manufactured by Netzsch, to explore the reaction characteristics in the temperature range from 15 °C to 65 °C. Figure 1 shows the specific heat power of the specimens at different temperatures. It is obvious, that higher temperatures accelerate the rate of reaction.

During the experiments, an incomplete curing was detected. This is due to the glass transition of the fully cured material at approximately 105 °C, which is far above the typical application temperature. For comparison the glass transition temperature of the liquid cement is about −50 °C and thus below the prescribed curing temperature. The reaction comes to a stop i.e., the material vitrifies, as soon as the glass transition temperature of the curing bone cement rises above the constant curing temperature [18–20]. To analyse this uncompleted curing, the sample was cooled down by 15 °C, heated up to 150 °C and cooled down to 20 °C three times, according to the temperature

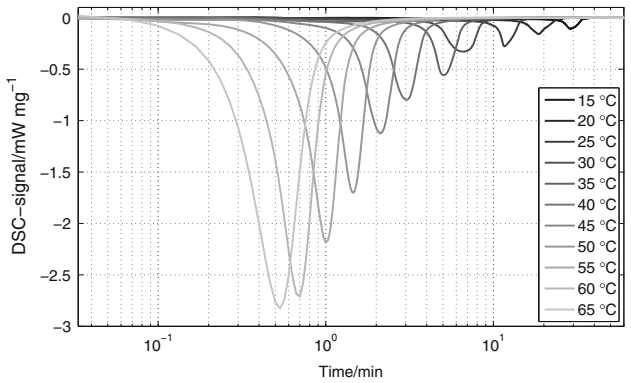

Fig. 1 DSC-signal of curing bone cements at different temperatures

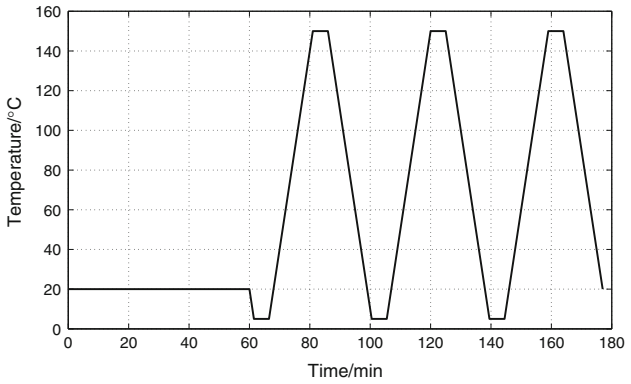

Fig. 2 Temperature profile of DSC experiments

profile in Fig. 2. Therewith it is possible to detect the remaining heat of reaction that is not set free during the isothermal phase. Figure 3 exemplary shows the DSC-signal of the heating ramps in the non-isothermal part of the calorimetric experiments (see also Fig. 2). Since the second and third ramp are identical, the polymerisation is finished after the first heating ramp. The remaining heat of reaction can thus be interpreted as the area between the first and the second heating ramp, assuming that the change of the specific heat with respect to the degree of cure is negligible. With the aid of this experimental data the temperature-dependent reaction kinetics as well as the enthalpy of reaction, including the phenomena of vitrification, can be quantified. The interested reader is referred to Kolmeder and Lion [21] for further details.

Specific heat

For thermomechanical finite element calculations the specific heat is an important material parameter. In general, the specific heat depends on temperature, degree of cure and on pressure, whereas the dependency on pressure is neglected in this study and therefore the specific heat under

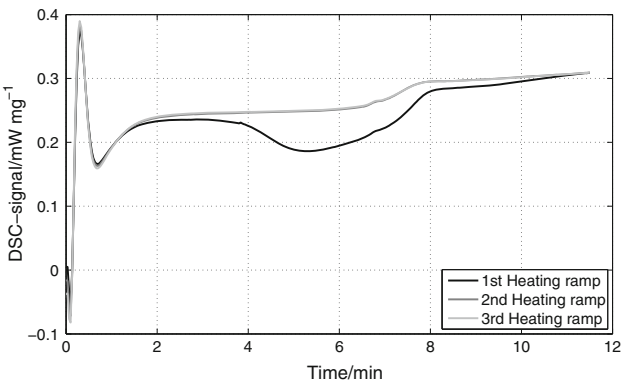

Fig. 3 DSC-signal for heating ramps in the non-isothermal part of the calorimetric measurements

constant pressure c_p is investigated. Differential scanning calorimetry was used to determine the specific heat in dependence on temperature for the uncured and the fully cured state.

Before measuring the sample at least three baselines were recorded to get accurate values. The DSC-signal of the bone cement specimen were evaluated and compared to sapphire standard measurements (see [22] for further details). In order to get a non curing mixture of bone cement and to measure the specific heat in the uncured state, a monomer without activator was used. Figure 4 shows the experimental results of the specific heat capacity measurements. In both cases, the specific heat capacity rises almost linearly with increasing temperature and shows nearly the same slope. The values for the cured state show clearly a glass transition in the region around 105 °C, which is conform with pure Polymethylmethacrylate. Moreover, Fig. 4 displays a slightly higher specific heat capacity for the uncured state compared to the cured state. A measurement beyond 80 °C in the uncured state was not possible, because polymerisation was thermally activated, although a monomer without an activator was used.

The results shown above give information about the initial and the final state of polymerising bone cement. However, no information about the behaviour of the specific heat during the polymerisation process can be gathered out of these experiments. Therefore, the temperature modulated differential scanning calorimetry (TMDSC) technique was used to investigate characteristics of the specific heat during curing. This technique allows for separating the heat power due to reversible and non-reversible processes by superposing a harmonic temperature load to the usual temperature program. The interested reader is referred to [23–26] for further details.

TMDSC-Experiments were performed at 15 °C and 20 °C with a superposed harmonic temperature load during the curing process. At higher temperatures the speed of the reaction is that fast, that the requirement for accurate

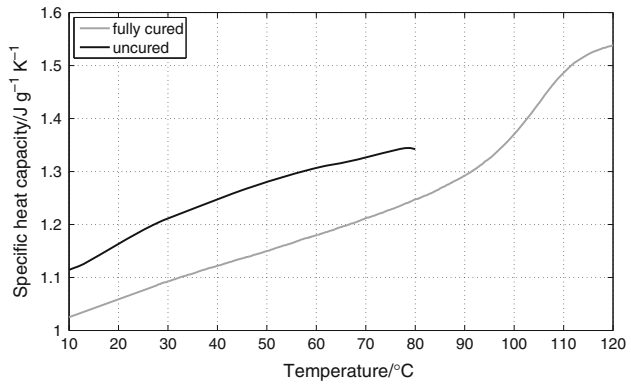

Fig. 4 Specific heat capacity of acrylic bone cement for the uncured and the fully cured state

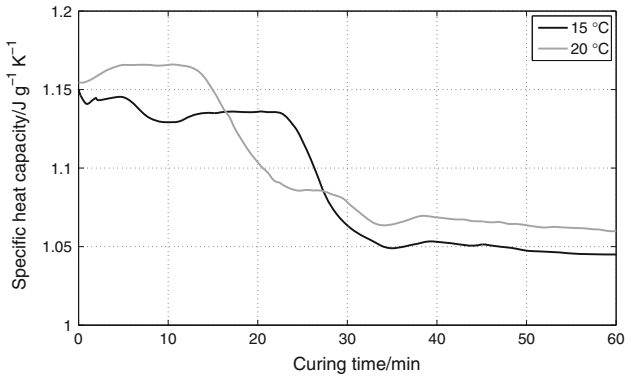

Fig. 5 Specific heat capacity of acrylic bone cement during curing at 15 °C and 20 °C

evaluation of TMDSC experiments could not be achieved any more. This requirement states, that the change in the degree of cure is small within one period of the superposed harmonic temperature load. An amplitude of 1 °C and a period of 50s were found to be appropriate parameters for the superposed harmonic temperature oscillation.

In Fig. 5 the course of the specific heat capacity is shown for isothermal curing at 15 °C and 20 °C. Comparing it with the reaction kinetics in Fig. 1, one can conclude that the specific heat capacity decreases with proceeding polymerisation. Furthermore, the temperature dependence of the reaction kinetics is visible in Fig. 5. Owing to the increasing mean chain length the overall mobility of the chains is handicapped. This phenomenon is directly linked to the decreasing specific heat capacity and thus to vitrification [2, 23].

Thermal conductivity

In addition to the specific heat capacity, thermomechanical coupled material models also contain the thermal conductivity as a material parameter. Within this study the thermal

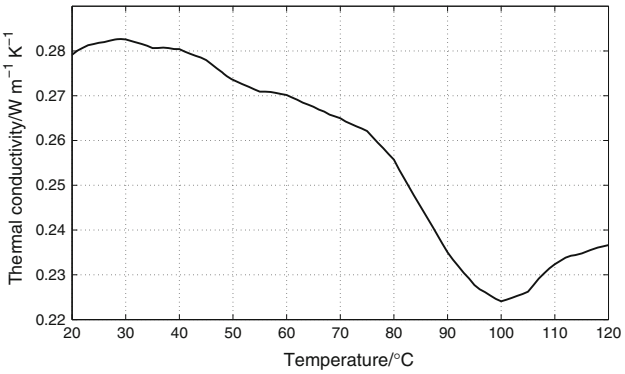

Fig. 6 Thermal conductivity of fully cured acrylic bone cement

conductivity of fully cured bone cement was analysed by means of a Netzsch LFA 427 Laser Flash apparatus in a temperature range from 20 °C to 120 °C. Usually, the thermal diffusivity is determined with the laser flash technique. Thermal conductivity λ and thermal diffusivity a are connected via the following relation:

$$\lambda = \rho c_p a \tag{1}$$

where ρ is the density (see Chemical shrinkage and thermal expansion) and c_p is the specific heat. For further details on the laser flash method see [27]. Figure 6 displays the results of the thermal conductivity measurement. In the region from 20 °C to 80 °C the thermal conductivity decreases almost linearly with increasing temperature. The relative change in this temperature interval is less than 10%. The stronger decrease from 80 °C to 100 °C and the increase above 100 °C can be explained by the glass transition of the thermal diffusivity and the specific heat, respectively. According to Risen and Schawe [28–30], the determination of the glass transition temperature by different thermal analysis techniques leads to different values, because the glass transition is a rate-dependent thermoviscoelastic phenomena [31].

So far no measurements were successful to determine the thermal diffusivity in the uncured state or during the curing process, because these techniques always base on a heat input into the material and therefore influence the reaction kinetics, which itself produces heat [32, 33].

Chemical shrinkage and thermal expansion

Like most curing polymers, acrylic bone cement shows also a chemical shrinkage. This physical property as well as the thermal expansion were measured using a self-built-up volumetric dilatometer. A precision balance ME235P from Sartorius was mounted over a Lauda cooling thermostat RE207 as shown in Fig. 7 and both devices were controlled by a computer routine. Using Archimedes principle the volume and the density can be measured in a

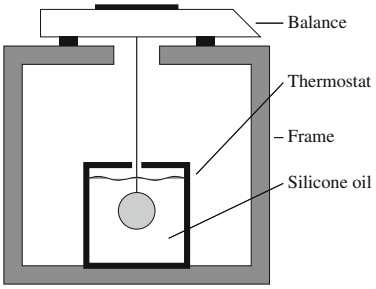

Fig. 7 Experimental setup for volumetric dilatometry

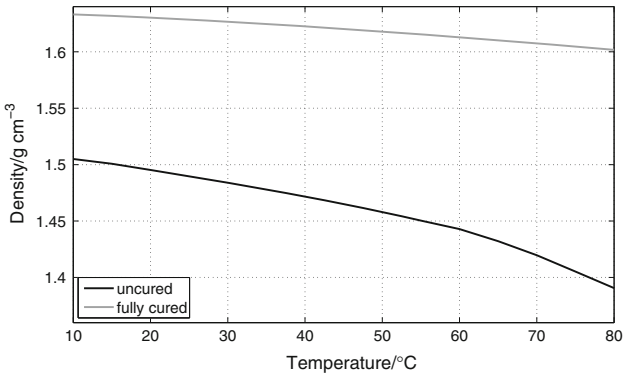

Fig. 8 Density of acrylic bone cement in the uncured and the fully cured state

temperature range from 5 °C to 120 °C. For further information on the device, sample preparation and measuring principle the interested reader is referred to [21]. At first, the thermal expansion behaviour of bone cement was investigated in the uncured and the fully cured state. Again, for the measurement in the uncured state, a monomer liquid without an activator was used. Two important things can be recognised in Fig. 8. First, the density in the fully cured state is approximately 10% above the density in the uncured state. That means the polymerisation process effects a chemical shrinkage of about 10%. Second, the thermal expansion i.e., the slope of the curves, is twice as high for the uncured state compared to the cured state. In addition, the density was also recorded for isothermal curing processes at temperatures from 12 °C to 62 °C with a step size of 5 °C. Figure 9 presents the density over time during the above mentioned experiments. At the very beginning i.e., up to 4 min, thermal expansion and chemical shrinkage are superposed, because the specimen was prepared at room temperature and the cooling thermostat was preconditioned at the test temperature. Nevertheless, it can be seen clearly that the shrinkage in volume follows the characteristics of the reaction kinetics. The density distribution at the end of the experiment is not only caused by the thermal expansion at different temperatures, but also

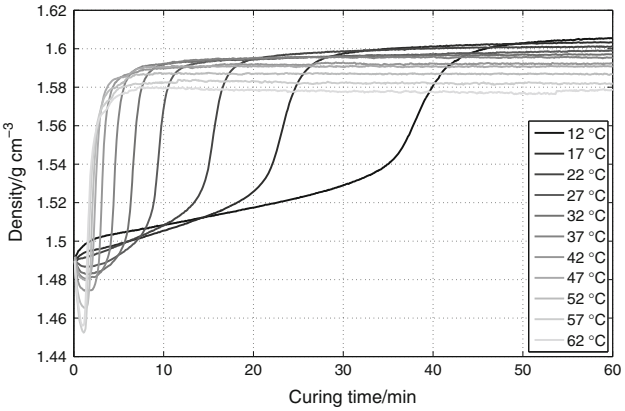

Fig. 9 Density of acrylic bone cement during isothermal curing processes at different temperatures

due to different degrees of cure due to incomplete polymerisation. On closer examination of Fig. 9 it can be seen, that the density is still rising after the material has been vitrified and the reaction is already diffusion controlled. The interested reader is refered to [21], where chemical shrinkage is compared with reaction kinetics of the examined material. For a deeper understanding of this delay of the shrinkage on the chemical conversion on basis of a kind of viscoelastic creep recovery response Maffezzoli and Terzi [34] as well as to Micelli and Maffezzoli [35] discuss these effects in detail.

Mechanical behaviour

A major challenge is the determination of the thermomechanical material behaviour, because acrylic bone cements undergo a phase transition from a viscoelastic fluid to a solid during polymerisation. That means that the mechanical material parameters vary within several orders of magnitude. In order to characterize the thermomechanical behaviour of curing materials, rheometers and especially rotational rheometers have turned out to be most appropriate [36, 37].

In this study a temperature controlled AR G2 Rheometer from TA Instruments, equipped with parallel plates of 8 mm in diameter, was used to investigate the thermoviscoelastic behaviour. The bone cement was brought in between the two plates, whereas the bottom plate is fixed and a harmonic torsional load was applied to the top plate. The torque response of the material is also harmonic but phase shifted with respect to the excitation. A distance of 1 mm between both plates was adjusted at the beginning of the experiment. But since the bone cement shrinks with proceeding polymerisation, the distance also decreases. Knowing the geometry as well as the loading and the response, the complex shear modulus, as well as its real part, the storage modulus, and its imaginary part, the loss

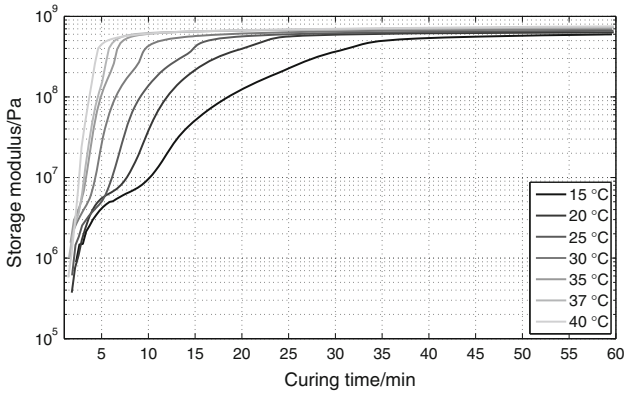

Fig. 10 Storage modulus of curing bone cement at a frequency of 1 Hz at different temperatures

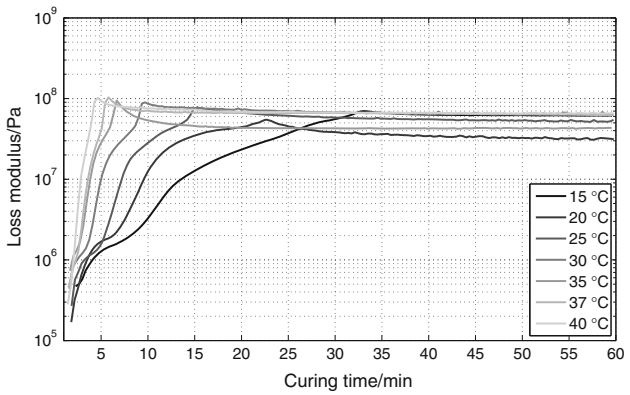

Fig. 11 Loss modulus of curing bone cement at a frequency of 1 Hz at different temperatures

modulus, can be calculated. For further details the interested reader is referred to [38]. Experiments were performed in a temperature range from 15 °C to 40 °C, in a frequency band from 1 Hz to 40 Hz and with a shear amplitude of 0.1%. The upper limit of the temperature range was 40 °C, because the sample started to polymerize during the preparation on the preconditioned plates at higher temperatures. The frequency band was limited by not getting enough data points at low frequencies (one data point per period only) and by the moment of inertia of the rheometer at high frequencies. Moreover, the shear amplitude was limited by the maximum detectable torque of the rheometer.

Figures 10 and 11 show exemplary the curves of storage and loss modulus during isothermal curing experiments at a frequency of 1 Hz and at different temperatures. Again, in both diagrams the influence of the temperature-dependent reaction kinetics is evident. Higher temperatures provoke a higher final storage modulus. This leads to the conclusion that the major degree of cure at higher temperatures has a greater influence than the softening due to higher

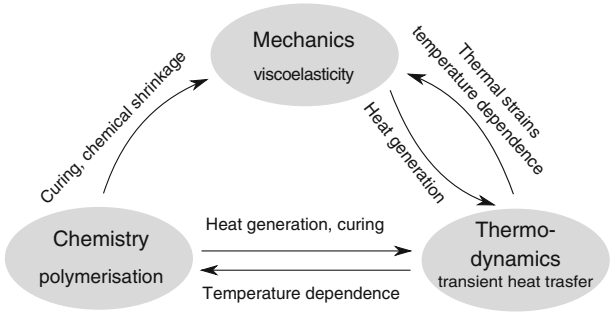

Fig. 12 Interaction of chemistry, mechanics and thermodynamics in curing phenomena

temperatures. The maxima in the loss modulus curves indicate the transition into the glassy state.

Material modelling

On the basis of the gathered thermophysical material properties in Experimental characterisation a material model is presented in this section, that is able to represent the thermomechanical-chemical coupling. This model was originally developed by Lion and Höfer [16] to describe the material behaviour of curing resins. Some minor modifications were made to the model to adapt it to acrylic bone cement material. Implemented in a finite element code the model is capable to solve for inhomogeneous temperature, degree of cure and stress fields, whereas the thermal, chemical and mechanical problem are mutually coupled.

These three different phenomena, that interact with each other, are pictured in Fig. 12. Since the polymerisation is a kind of driving force for all the other material parameters, it is reasonable to model the reaction kinetics first.

Reaction kinetics

For curing polymers it is common to define the degree of cure $q(t)$ as the relation of the cumulative released heat of the polymerisation $H(t)$ with respect to the total reaction enthalpy H_u.

$$q(t) = \frac{H(t)}{H_u} \quad \text{with} \quad H(t) = \int_0^t \left(\frac{dQ}{d\bar{t}}\right) d\bar{t} \tag{2}$$

$\frac{dQ}{d\bar{t}}$ is the heat power of the reaction at time $\bar{t}$. An appropriate model to describe the progress of polymerisation of bone cement is the single step evolution equation introduced by Kamal and Sourour [39, 40]. The calculation of an induction time, as proposed by Maffezzoli an others [2, 41, 42], was neglected, since bone cements, that are designed especially for vertebroplasty, show a very

spontaneous reaction behaviour and, hence, most of the induction time is consumed by the sample preparation time. To account for incomplete curing i.e., the vitrification, due to diffusion control, it is necessary to extend the original evolution equation by a diffusion coefficient f_D, which was proposed by Fournier [43].

$$\frac{dq}{dt} = (K_1 + K_2 \cdot q^{\alpha})(1-q)^{\beta} f_D(q) \tag{3}$$

with

$$f_D(q) = \left[\frac{2}{1+\exp(\frac{q-q_{end}}{b})} - 1\right] \tag{4}$$

K_1 and K_2 are temperature-dependent material parameters that show an Arrhenius behaviour:

$$K_i = K_{i0} \exp\left(\frac{-E_i}{RT}\right) \quad i = 1,2 \tag{5}$$

The parameters K_{10}, K_{20}, E_1 and E_2 in Eq. 5 have to be fitted to the experimental data in Reaction kinetics. $R = 8.314$ J/molK is the universal gas constant. α, β and b in Eqs. 3 and 4 are further material parameters and q_{end} is the maximum degree of cure that can be attained at a certain curing temperature. Some studies (see for example [2, 3, 41, 42]) omit the parameter K_1. However, they have to prescribe $q \neq 0$ as an initial condition. The dependence of the maximum degree of cure on the curing temperature is calculated with means of a modified DiBenedetto equation (see [2, 18, 20]), which is only valid in the application temperature range of acrylic bone cements i.e., 15 °C to 80 °C:

$$\frac{T_g(q) - T_{g,0}}{T_{g,1} - T_{g,0}} = \kappa q + \xi \tag{6}$$

$T_g(q)$ is the glass transition temperature at a degree of cure q, $T_{g,0}$ is the glass transition temperature at a degree of cure $q = 0$ and $T_{g,1}$ is the glass transition temperature at a degree of cure $q = 1$ in Eq. 6. κ and ξ are further material parameters. Rearranging of Eq. 6 leads to:

$$q_{end} = \frac{f(T) - \xi}{\kappa} \tag{7}$$

with

$$f(T) = \frac{T_{iso} + \Delta T - T_{g,0}}{T_{g,1} - T_{g,0}} \tag{8}$$

and

$$T_g(q_{end}) = T_{iso} + \Delta T \tag{9}$$

For isothermal polymerisation below the maximal attainable glass transition temperature $T_{g,1}$ of the fully cured bone cement, a glass transition temperature of $T_g(q_{end})$ is reached. This glass transition temperature

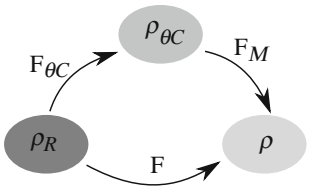

Fig. 13 Multiplicative split of the deformation gradient in a mechanical and thermochemical part

$T_g(q_{end})$ is approximately $\Delta T = 20\,°C$ higher than the isothermal curing temperature T_{iso} [18, 20]. For further information the interested reader is referred to [21].

Decomposition of the deformation gradient and the free energy

The basic idea of the material model is to distinguish between pure mechanical-induced strains i.e., caused by external forces, surface forces or body forces, and strains that are induced only by thermal expansion or chemical shrinkage. Therefore, the deformation gradient is split into a mechanical and a thermochemical part, according to Fig. 13 and Eq. 10.

$$\mathbf{F} = \mathbf{F}_M \mathbf{F}_{\theta C} \tag{10}$$

The free energy is chosen as thermodynamic potential and is additively split into a mechanical and a thermochemical part.

$$\psi = \psi_M + \psi_{\theta C} \tag{11}$$

Enthalpy of reaction and specific heat

For representing the thermochemical properties of curing materials usually the enthalpy is taken as a thermodynamic potential, because calorimetric measurements are usually performed at constant pressure. In general, the enthalpy of a curing material is a function of stress $\mathbf{T}$, temperature θ and degree of cure q

$$h = h(\mathbf{T}, \theta, q) \tag{12}$$

In the following, the dependence of the enthalpy on stress will be neglected i.e., at first only states under constant stress ($\dot{\mathbf{T}} = 0$) and therefore only the thermochemical part of the enthalpy will be considered. The complete material model accounts for this dependence in the mechanical part of the free energy ψ_M (see Equation of heat conduction). These considerations yield for the rate of enthalpy

$$\dot{h} = \frac{\partial h}{\partial \theta}\dot{\theta} + \frac{\partial h}{\partial q}\dot{q} \tag{13}$$

This rate of enthalpy can be registered by differential scanning calorimetry. The experiments in Reaction kinetics and Specific heat suggest to model the enthalpy linearly

dependent on the degree of cure and quadratically on temperature:

$$h(\theta, q) = h_F(\theta)(1-q) + h_S(\theta)q \tag{14}$$

$$h_F(\theta) = h_{F0} + a_F(\theta - \theta_0) + \frac{1}{2}b_F(\theta - \theta_0)^2 \tag{15}$$

$$h_S(\theta) = h_{S0} + a_S(\theta - \theta_0) + \frac{1}{2}b_S(\theta - \theta_0)^2 \tag{16}$$

Herein h_F is the enthalpy of the uncured and h_S the enthalpy of the fully cured material. h_{F0}, h_{S0}, a_F, a_S, b_F and b_S are material parameters to be identified. Therewith the enthalpy of reaction of a completely proceeded polymerisation is:

$$\Delta h(\theta) = h_S(\theta) - h_F(\theta) = h_{S0} - h_{F0} + (a_S - a_F)(\theta - \theta_0) + \frac{1}{2}(b_S - b_F)(\theta - \theta_0)^2 \tag{17}$$

The difference $h_{S0} - h_{F0}$ can be determined from calorimetric measurements, if the degree of cure is known. For identifying the other material parameters the measurements of the specific heat are more appropriate (see Specific heat). The specific heat at constant pressure ($\dot{\mathbf{T}} = 0$) is defined as:

$$c_p := \frac{\partial h}{\partial \theta} \tag{18}$$

Using the Eqs. 14, 15 and 16 the specific heat adds up to:

$$c_p(\theta, q) = \frac{\partial h_F}{\partial \theta}(1-q) + \frac{\partial h_S}{\partial \theta}q = c_p^F(\theta)(1-q) + c_p^S(\theta)q \tag{19}$$

$$c_p^F(\theta) = \frac{\partial h_F}{\partial \theta} = a_F + b_F(\theta - \theta_0) \tag{20}$$

$$c_p^S(\theta) = \frac{\partial h_S}{\partial \theta} = a_S + b_S(\theta - \theta_0) \tag{21}$$

Equations 17 and 19 show that a dependence of the specific heat on the degree of cure (i.e., $c_p^F \neq c_p^S$) involves a dependence of the enthalpy of reaction on temperature.

Thermal conductivity

The experiments in Thermal conductivity propose a linearly dependent modelling of the thermal conductivity λ within the temperature range from 20 °C to 80 °C

$$\lambda(\theta) = \lambda_0 + c_\lambda(\theta - \theta_0) \tag{22}$$

Whereas λ_0 and c_λ are material parameters to be identified. The modelling of the thermal conductivity can be extended similar to the characterisation of the specific heat in Eq. 19 when the influence of the degree of cure on the thermal conductivity is known.

Chemical shrinkage and thermal expansion

Acrylic bone cement is an isotropic material. Therefore, the following function is chosen for the thermochemical part of the deformation gradient:

$$\mathbf{F}_{\theta C} = \varphi(\theta, q)^{1/3}\mathbf{1} \tag{23}$$

The function φ describes the volumetric strains with respect to temperature and degree of cure. The results from Chemical shrinkage and thermal expansion motivate a linear dependence of density on degree of cure and temperature. In addition, the coefficient of linear thermal expansion should also change with proceeding polymerisation. For simplicity, the phenomen of volume relaxation recovery (see [34, 35] has been neglected. This leads to the following equation for the description of thermal and chemical strains:

$$\varphi(\theta, q) = 1 + (\zeta + \Delta\zeta q(t))(\theta - \theta_0) + \varepsilon q(t) \tag{24}$$

Herein ζ is the coefficient of linear thermal expansion in the uncured state, $\Delta\zeta$ is the change of the coefficient of linear thermal expansion from the uncured to the fully cured state and ε is the chemical shrinkage. These coefficients have to be adapted to experimental data.

Mechanical behaviour

The basis for modelling the mechanical material behaviour is the mechanical deformation gradient $\mathbf{F}_M$ that can be derived by combining Eqs. 10 and 23 as:

$$\mathbf{F}_M = \frac{1}{\varphi(\theta, q)^{1/3}}\mathbf{F} \tag{25}$$

In a first approach bone cement is modelled mechanically incompressible in this study. Hence, the determinant of the deformation gradient reads as:

$$\det \mathbf{F}_M = 1 \tag{26}$$

and the Cauchy stresstensor $\mathbf{T}$ is given by:

$$\mathbf{T} = -p\mathbf{1} + \mathbf{S} \tag{27}$$

$\mathbf{S}$ is the deviatoric stress that has to be evaluated by means of constitutive relations, and $-p\mathbf{1}$ is the resulting volumetric stress, because of incompressibility. As the rheologic experiments indicated a viscoelastic material behaviour, a constitutive relation of finite viscoelasticity is used for the deviatoric stress part. The rheological behaviour of a Maxwell element is the basis for the constitutive law. In order to represent the actual material behaviour more accurately, not only one Maxwell is used but a chain of parallel connected elements according to Fig. 14.

Hence, the constitutive relation between stress and strain reads as

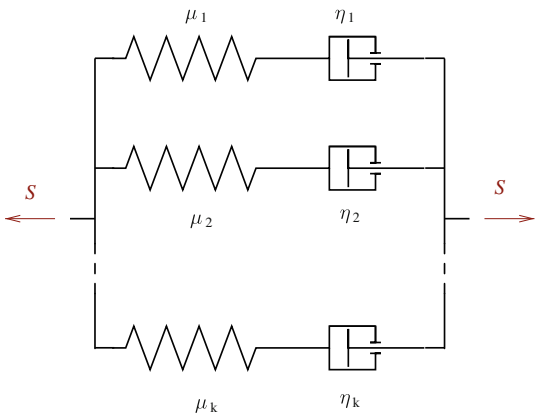

Fig. 14 Chain of Maxwell elements

$$\mathbf{S} = \frac{1}{\varphi}\sum_{k=1}^{N}\mathbf{S}_k \tag{28}$$

$$\overset{\triangledown}{\mathbf{S}}_k = 2\rho_R\mu_k\mathbf{D}_M - \frac{1}{\tau_k}\mathbf{S}_k \tag{29}$$

Whereas ρ_R is the density of the reference configuration, μ_k are the elastic parameters and τ_k the element-specific relaxation times that have to be determined from the experimental data in Mechanical behaviour. Usually, the viscosity $\eta_k = \tau_k\mu_k$ is introduced to replace the relaxation times τ_k. The mechanical strain rate tensor $\mathbf{D}_M$ is defined as:

$$\mathbf{D}_M = \frac{1}{2}\left(\dot{\mathbf{F}}_M\mathbf{F}_M^{-1} + \mathbf{F}_M^{T-1}\dot{\mathbf{F}}_M^{T}\right) \tag{30}$$

The expression $\overset{\triangledown}{\mathbf{S}}_k$ corresponds to a covariant Oldroyd derivative (see [44–46]) of the deviatoric stress and is calculated with the definition of the velocity gradient $\mathbf{L}_M$ ($\mathbf{L}_M = \dot{\mathbf{F}}_M\mathbf{F}_M^{-1}$) as follows:

$$\overset{\triangledown}{\mathbf{S}}_k = \dot{\mathbf{S}}_k - \mathbf{L}_M\mathbf{S}_k - \mathbf{S}_k\mathbf{L}_M^{T} \tag{31}$$

To take into account the temperature and degree of cure dependence of the material behaviour a non linear temperature and degree of cure-dependent viscosity function is introduced:

$$\eta_k = \eta_k(\theta, q) \tag{32}$$

Equation of heat conduction

The equation of heat conduction is an essential part in the presented model. For inhomogeneous problems mechanical dissipation as well as exothermal reaction lead to temperature increase. Furthermore, mechanical properties and the reaction kinetics are highly temperature sensitive.

Since the free energy is used as thermodynamic potential for the material model, but in the thermochemical part of the model only the enthalpy is present, a conjunction has to be established for these thermodynamic properties. Therefore the first law of thermodynamics is evaluated to derive the equation of heat conduction.

$$\rho_R\dot{e} = -\mathrm{div}\,\vec{\mathbf{q}} + \tilde{\mathbf{T}}\cdot\dot{\mathbf{E}} + \rho_R r \tag{33}$$

ρ_R is the mass density of the reference configuration, $\dot{e}$ is the rate of internal energy, $\vec{\mathbf{q}}$ is the heat flux vector and r volumetric distributed heat sources or sinks. The stress power $\tilde{\mathbf{T}}\cdot\dot{\mathbf{E}}$, the scalar product of the second Piola Kirchhoff stresstensor $\tilde{\mathbf{T}}$ and the time derivative of the Green straintensor $\mathbf{E}$ (see [44, 45]) can be calculated from the constitutive material functions in Eqs. 10 and 27. Volumetric distributed heat sources are not present in the observed curing reaction ($r = 0$). To calculate the heat flux vector Fourier's law of heat conduction is used:

$$\vec{\mathbf{q}} = -\lambda\ \mathrm{grad}\ \theta \tag{34}$$

Under consideration of Eq. 11 and the Legendre transformation $e = \psi + \theta\, s$ (see also [47, 48]) as well as the split of the entropy in a mechanical and a thermochemical part $s = s_M + s_{\theta C}$, the rate of the internal energy $\dot{e}$ is given by:

$$\dot{e} = (\dot{\psi}_M + \dot{\psi}_{\theta C} + \dot{\theta}s_M + \dot{\theta}s_{\theta C} + \theta\dot{s}_M + \theta\dot{s}_{\theta C}) \tag{35}$$

Furthermore, for the entropy s is valid:

$$s = -\frac{\partial\psi}{\partial\theta} \tag{36}$$

and therefore the rate of thermochemical entropy $\dot{s}_{\theta C}$ reads as

$$\dot{s}_{\theta C} = -\frac{\partial^2\psi_{\theta C}}{\partial\theta^2}\dot{\theta} - \frac{\partial^2\psi_{\theta C}}{\partial\theta\partial q}\dot{q} \tag{37}$$

with $s_{\theta C} = s_{\theta C}(\theta, q)$ and the rate of the thermochemical free energy $\dot{\psi}_{\theta C}$ reads as

$$\dot{\psi}_{\theta C} = \frac{\partial\psi_{\theta C}}{\partial q}\dot{q} + \frac{\partial\psi_{\theta C}}{\partial\theta}\dot{\theta} \tag{38}$$

with $\psi_{\theta C} = \psi_{\theta C}(\theta, q)$ and under consideration of Eqs. 36, 37 and 38, the rate of internal energy is given by

$$\dot{e} = (\dot{\psi}_M + \dot{\theta}s_M + \theta\dot{s}_M) - \theta\frac{\partial^2\psi_{\theta C}}{\partial\theta^2}\dot{\theta} + \frac{\partial}{\partial q}\left(\psi_{\theta C} - \theta\frac{\partial\psi_{\theta C}}{\partial\theta}\right)\dot{q} \tag{39}$$

Equation 39 can be further summarized if the relation $h = \psi_{\theta C} - \theta\, s_{\theta C}$ ($h \hat{=} h_{\theta C}$) (see also [47, 48]) and the definition (18) are considered and reads as

$$\dot{e} = (\dot{\psi}_M + \dot{\theta}s_M + \theta\dot{s}_M) - c_p\dot{\theta} + \frac{\partial h}{\partial q}\dot{q} \tag{40}$$

The mechanical part of the free energy can be calculated directly from the relaxation functions (see [49, 50])

$$\psi_M = -\int_{-\infty}^{z} \sum_{k=1}^{N} \mu_k \exp^{-\frac{z-s}{\tau_k}} \frac{\mathrm{d}}{\mathrm{d}s} tr(\mathbf{e}_M)\mathrm{d}s \tag{41}$$

Whereas $tr(\mathbf{e}_M)$ is the trace of the mechanical part of the Piola strain tensor. Therewith, all physical variables to solve the equation of heat conduction, are known.

Parameter identification

The developed material functions in Material modelling were adapted to the experimental data sets presented in Experimental characterisation by deterministic methods that are available in the program package MATLAB. In particular, the non linear least square algorithm "lsqnonlin" was used.

Reaction kinetics

As the degree of cure acts as an internal variable in the material model, the evolution Eq. 3 has to be identified first. The results of the identification of the evolution equation can be seen in Table 1 and Fig. 15.

Enthalpy and specific heat

In chapter 4.3, it was shown that the dependence of the specific heat on the degree of cure has a direct impact on the dependence of the reaction enthalpy on temperature. The parameters a_F, a_S, b_F and b_S (see Eqs. 20 and 21) could be determined very accurately from measurements of the specific heat in the uncured and the fully cured state (see Fig. 4). The reference temperature θ_0 was chosen to be the body temperature of 37 °C. Table 2 shows the identified parameters.

Table 1 Identified material parameters of the kinetic evolution equation

Parameter	Identified value
κ	2.5021
ξ	1.3592
$T_{g,0}$	−50 °C
$T_{g,1}$	105 °C
K_{10}	1.792×10^{10}
K_{20}	3.234×10^{6}
E_1	7.964×10^{4} J/mol
E_2	4.571×10^{4} J/mol
α	2.05
β	0.95
b	0.1917

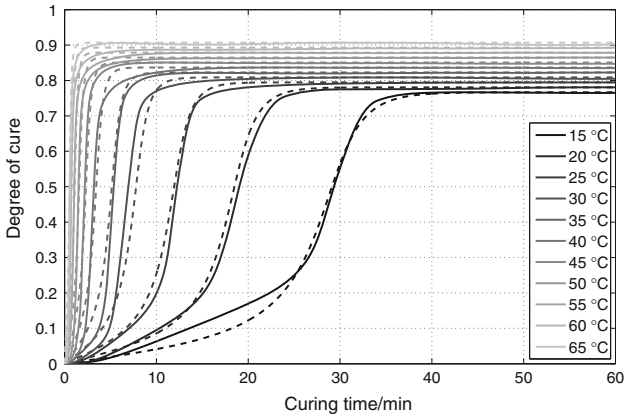

Fig. 15 Adaptation of the progress of the degree of cure of acrylic bone cements; Measurement(—) and simulation (- -) with identified parameters

Table 2 Identified material parameters of the constitutive equations for enthalpy of reaction and specific heat

Parameter	Identified value
a_F	1.226 J/gK
b_F	0.003288 J/gK^2
a_S	1.112 J/gK
b_S	0.003011 J/gK^2
$h_{S0} - h_{F0}$	−100 J/g

The comparison between measurement and simulation with the identified material parameters for isothermal polymerisation, using the example of specific heat and heat release, is shown in Figs. 16 and 17, respectively.

Thermal conductivity

According to Eq. 22, the temperature dependent thermal conductivity has been adapted to experimental data in the relevant temperature interval from 20 °C to 80 °C. Table 3 displays the identified parameters for a reference temperature of 37 °C.

Chemical shrinkage and thermal expansion

In order to determine the material parameters of Eq. 24, that describes thermal strains due to chemical shrinkage and thermal expansion, measurements of density in the uncured state (see Fig. 8) and shrinkage measurements during isothermal polymerisation (see Fig. 9) were used. Because isothermal curing measurements showed a temperature compensation during the first 4 min, these values were not considered for parameter identification. Table 4 shows the identified parameters. Figure 18 compares measurement and simulation of thermochemical strains during isothermal

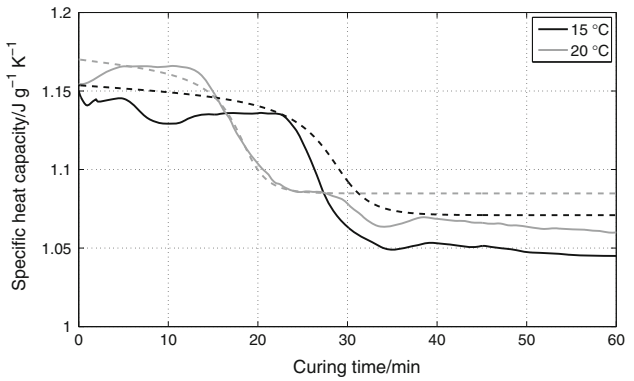

Fig. 16 Comparison between measurement and simulation of specific heat capacity for isothermal polymerisation; measurement (—) and simulation (- -) with identified parameters

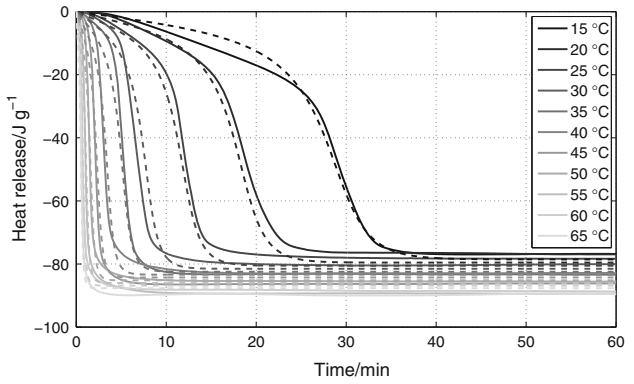

Fig. 17 Comparison between measurement and simulation of released heat for isothermal polymerisation; measurement (—) and simulation (- -) with identified parameters

Table 3 Identified material parameters of the constitutive equation for thermal conductivity

Parameter	Identified value
λ_0	0.2788 W/mK
c_λ	−0.000423 W/mK^2

Table 4 Identified material parameters of the constitutive equation for chemical shrinkage and thermal expansion

Parameter	Identified value
ζ	0.000928 1/°C
$\Delta\zeta$	−0.000367 1/°C
ε	−0.090602

polymerisation. The results of the parameter identification evidence that the thermochemical material behaviour can be well described by using the degree of cure as an internal variable.

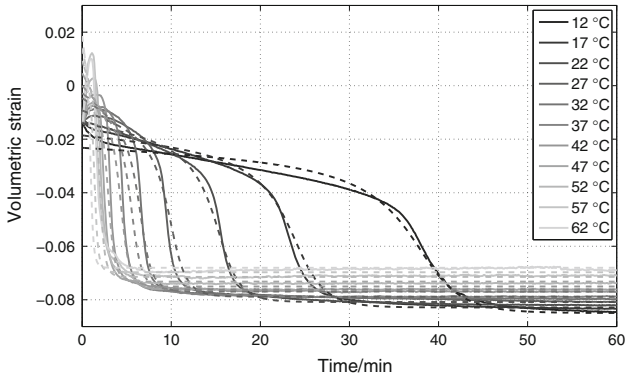

Fig. 18 Comparison between measurement and simulation of thermochemical strains during isothermal polymerisation; measurement (—) and simulation (- -) with identified parameters

Table 5 Identified material parameters for thermomechanical evolution equations

Parameter	Identified value
$\eta_{1,0}$	1.0129×10^{18} m^2/s^3
$\eta_{2,0}$	1.1654×10^{18} m^2/s^3
$\eta_{3,0}$	5.8647×10^{17} m^2/s^3
$\eta_{4,0}$	8.7731×10^{16} m^2/s^3
$\eta_{5,0}$	3.4562×10^{15} m^2/s^3
$\eta_{6,0}$	8.7150×10^{13} m^2/s^3
$\eta_{7,0}$	2.1076×10^{13} m^2/s^3
$\eta_{8,0}$	8.5948×10^{12} m^2/s^3
$\eta_{9,0}$	3.7677×10^{12} m^2/s^3
$\eta_{10,0}$	1.4080×10^{12} m^2/s^3
$\eta_{11,0}$	3.1222×10^{11} m^2/s^3
$\eta_{12,0}$	1.6082×10^{10} m^2/s^3
$\eta_{13,0}$	5.8926×10^{7} m^2/s^3
$\eta_{14,0}$	3.2149×10^{5} m^2/s^3
$\eta_{15,0}$	2.6234×10^{5} m^2/s^3
μ_1	157.0083 m^2/s^2
μ_2	260.4786 m^2/s^2
μ_3	432.1372 m^2/s^2
μ_4	716.9209 m^2/s^2
μ_5	1.1894×10^{3} m^2/s^2
μ_6	1.9732×10^{3} m^2/s^2
μ_7	3.2736×10^{3} m^2/s^2
μ_8	5.4309×10^{3} m^2/s^2
μ_9	9.0099×10^{3} m^2/s^2
μ_{10}	1.4948×10^{4} m^2/s^2
μ_{11}	2.4798×10^{4} m^2/s^2
μ_{12}	4.1140×10^{4} m^2/s^2
μ_{13}	6.8252×10^{4} m^2/s^2
μ_{14}	1.1323×10^{5} m^2/s^2
μ_{15}	1.8785×10^{5} m^2/s^2
a_v	0.00944 1/°C^2
b_v	0.5184 1/°C
a_t	0.029 1/°C
b_t	0.4943
c_v	14.49

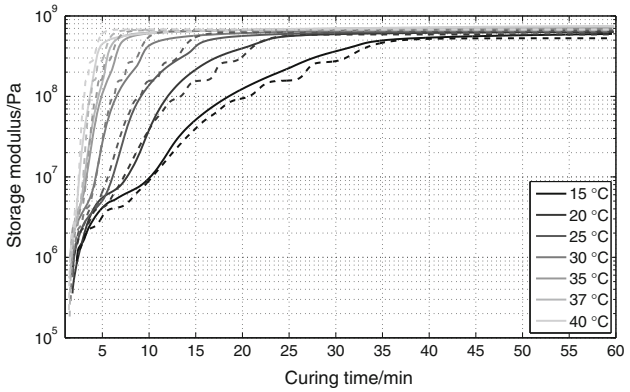

Fig. 19 Comparison between measurement and simulation of storage modulus during isothermal curing at different temperatures and at a frequency of 1 Hz; measurement (—) and simulation (- -) with identified parameters

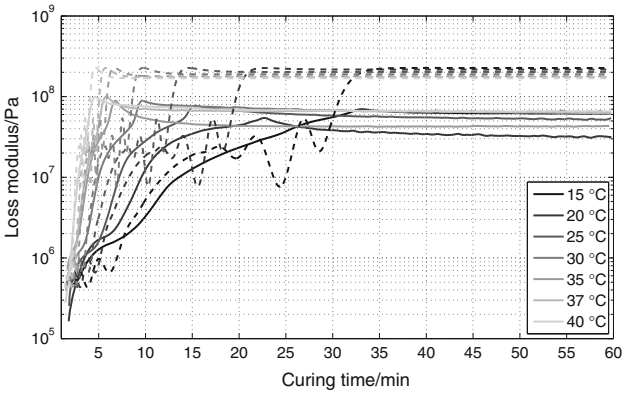

Fig. 20 Comparison between measurement and simulation of loss modulus during isothermal curing at different temperatures and at a frequency of 1 Hz; measurement (—) and simulation (- -) with identified parameters

Thermomechanical behaviour

An appropriate linearisation of the constitutive material functions (see [15]) leads to explicit Eqs. 43 and 44 for storage G' and loss modulus G'' of the complex shear modulus $G^* = G' + iG''$ for mono frequent harmonic loads with a frequency of $f = 2\pi\omega$.

$$\tau = G^*(\omega, q, \theta)\Delta\gamma \tag{42}$$

$$G' = \frac{1}{\varphi}\sum_{k=1}^{N}\frac{\rho_R\mu_k(\omega\eta_k/\mu_k)^2}{(\omega\eta_k/\mu_k)^2+1} \tag{43}$$

$$G'' = \frac{1}{\varphi}\sum_{k=1}^{N}\frac{\rho_R\mu_k(\omega\eta_k/\mu_k)}{(\omega\eta_k/\mu_k)^2+1} \tag{44}$$

The viscosities η_k are dependent on the degree of cure and temperature, as indicated in Eq. 32:

$$\eta_k = \eta_{k,0}q^{\upsilon}10^{\iota} \tag{45}$$

Herein υ and ι are functions of temperature

$$\upsilon(\theta) = a_\upsilon(\theta-\theta_0)^2 + b_\upsilon(\theta-\theta_0) + c_\upsilon \tag{46}$$

$$\iota(\theta) = a_\iota(\theta-\theta_0) + b_\iota \tag{47}$$

The constitutive Eqs. 43, 45, 46 and 47 were identified for a number of $k = 15$ Maxwell elements, using the experimental data from Fig. 10. Table 5 displays the identified material parameters. Figure 19 and 20 show that the thermomechanical material behaviour during polymerisation can be represented well by the presented model. As only the storage modulus is considered in the least square function, the deviation between measurement and simulation of the loss modulus is quite high. An increase in the number of Maxwell elements probably leads to an improvement of the adaptation.

Conclusions

A detailed experimental characterisation of the thermophysical properties of a curing commercial acrylic bone cement was performed within the temperature range relevant for application. On the basis of this experimental data pool a three dimensional model for curing resins was adapted and the material parameters were identified. The model is able to represent all observed thermochemical and thermomechanical effects. Especially the incomplete curing due to diffusion control and the chemical shrinkage during the polymerisation is taken into account. Moreover, the mechanical behaviour is modelled viscoelastic and the thermodynamic properties specific heat capacity and enthalpy are modelled to depend on both, temperature and degree of cure. However, the thermal conductivity needs to be measured in the uncured state and during polymerisation to calculate accurate temperature distributions. Aside, the representation of the loss modulus in the thermomechanical behaviour can be improved.

Further steps are the implementation of the presented model into a finite element code to calculate temperature distributions, inhomogeneous field of degree of cure and mechanical stresses. Moreover, the model should be calibrated on example problems, where both, experimental and numerical results, are compared. The goal is to apply the model on complex geometries like they appear during the thermal setting of acrylic bone cements in the vertebroplastic process. In combination with a parameter study these simulations can help to avoid failure and potential risks that are always associated with such a minimal invasive surgery. In addition, a deeper understanding of the processes itself, that takes place within the human vertebra during vertebroplasty, can be attained.

Acknowledgements The authors would like to thank the German Research Foundation DFG for support of this study.

References

1. Mazzullo S, Paolini M, Verdi C. Numerical simulation of thermal bone necrosis during cementation of femoral prostheses. J Math Biol. 1991;29:475–94.
2. Maffezzoli A, Ronca D, Guida G, Pochini I, Nicolais L. In-situ polymerization behaviour of bone cements. J Mater Sci Mater Med. 1997;8:75–83.
3. Lingois P, Berglund L, Maffezzoli A. Chemically induced residual stresses in dental composites. J Mater Sci. 2003;38:1321–31.
4. Briscoe A, New A. Polymerisation stress modelling in acrylic bone cement. J Biomech. 2010;43:978–83.
5. Perez MA, Nuno N, Madrala A, Garcia-Aznar JM, Doblare M. Computational modelling of bone cement polymerization: temperature and residual stresses. Comput Biol Med. 2009;39:751–9.
6. Beaudoin AJ, Mihalko WM, Krause WR. Finite element modelling of polymethylmethacrylate flow through cancellous bone. J Biomech. 1991;24(2):127–36.
7. Baroud G, Yahia FB. A finite element rheological model for polymethylmethacrylate flow: analysis of the cement delivery in vertebroplasty. J Eng Med. 2004;218:331–8.
8. Baroud G, Bohner M, Heini PF, Steffen T. Injection of biomechanics of bone cements used in vertebroplasty. Biomed Mater Eng. 2004;14:487–504.
9. Baroud G, Vant C, Giannitsios D, Bohner M, Steffen T. Effect of vertebral shell on injection pressure and intravertebral pressure in vertebroplasty. Spine. 2004;30:68–74.
10. Baroud G, Crookshank M, Bohner M. High-viscosity cement significantly enhances uniformity of cement filling in vertebroplasty: an experimental model and study on cement leakage. Spine. 2004;31:2562–8.
11. Srimongkol S, Wiwatanapataphee B, Wu YH. Computer simulation of polymethylacrylate bone cement flow through femoral canal and cancellous bone. Aust New Zealand Ind Appl Math J. 2005;47:C404–18.
12. Choon Meng JT. Patient specific finite volume modeling for intraosseous PMMA cement flow simulation in vertebral cancellous bone. PhD thesis, National University of Singapore. 2007.
13. Baroud G, Nemes J, Heini PF, Steffen T. Load shift of the intervertebral disc after a vertebroplasty: a finite element study. Eur Spine J. 2004;12:421–6.
14. Rohlmann A, Zander T, Jony WU, Weber U, Bergmann G. Einfluss der Wirbelkrpersteifigkeit auf den intradiskalen druck. Biomed Tech. 2005;50:148–52.
15. Lion A, Yagimli B, Baroud G, Görke U. Constitutive modelling of PMMAbased bone cement: a functional model of viscoelasticity and its approximation for time domain investigations. Arch Mech. 2008;60:221–42.
16. Lion A, Höfer P. On the phenomenological representation of curing phenomena in continuum mechanics. Arch Mech. 2007;59:59–89.
17. Drebushchak VA. From electrical analog to thermophysical modeling of DSC. J Therm Anal Calorim. 2010. doi:10.1007/s109730 1012003.
18. Schawe JEK. A description of chemical and diffusion control in isothermal kinetics of cure kinetics. Thermochim Acta. 2002;388:299–312.
19. Blumenstock T. Analyse der Eigenspannungen während der Aushärtung von Epoxidharzmassen. PhD thesis, Universität Stuttgart. 2003.
20. Wenzel M. Spannungsbildung und Relaxationsverhalten bei der Aushärtung von Epoxidharzen. Technische Universität Darmstadt. 2005.
21. Kolmeder S, Lion A. On the thermomechanical-chemically coupled behavior of acrylic bone cements: experimental characterization of material behavior and modeling approach. Tech Mech. 2010;30:195–202.
22. O'Neill MJ. Measurement of specific heat functions by differential scanning calorimetry. Anal Chem. 1996;38:1331–6.
23. Van Assche G, Van Hemelrijck A, Rahier H, Van Mele B. Modulated differential scanning calorimetry: isothermal cure and vitrification of thermosetting systems. Thermochim Acta. 2004; 268:121–42.
24. Lion A, Yagimli B. Differential scanning calorimetry—continuum mechanical considerations with focus to the polymerisation of adhesives. Z Angew Math Mech. 2008;88:388–402.
25. Shanks RA, Gunaratne LMWK. Comparison of reversible melting behaviour of poly(3-hydroxybutyrate) using quasi-isothermal and other modulated temperature differential scanning calorimetry techniques. J Therm Anal Calorim. 2011. doi:10.1007/s 1097301112835.
26. Gracia-Fernández C, Tarró-Saavedra J, López-Beceiro J, Gómez-Barreiro S, Naya S, Artiaga R. Temperature modulation in PDSC for monitoring the curing under pressure. J Therm Anal Calorim. 2011. doi:10.1007/s1097301113618.
27. Sato Y, Taira T. The studies of thermal conductivity in GdVO4, YVO4, and Y3Al5O12 measured by quasi-onedimensional flash method. Opt Exp. 2006;14:10528–36.
28. Moynihan CT, Easteal AJ, Wilder J, Tucker J. Dependence of the glass transition temperature on heating and cooling rate. J Phys Chem 1974;78:2673–7.
29. Risen R, Schawe JKE. Die Glasübergangstemperatur gemessen mit verschiedenen TA Techniken. Teil 1: Übersicht. UserCom. 2003;17:1–4.
30. Risen R, Schawe JKE. Die Glasübergangstemperatur gemessen mit verschiedenen TA Techniken, Teil 2: ermittlung der glasübergangstemperatur. UserCom. 2003;18:1–5.
31. Lion A, Liebl C, Kolmeder S, Peters J. Representation of the glass-transition in mechanical and thermal properties of glass-forming materials: a three-dimensional theory based on thermodynamics with internal state variables. J Mech Phys Solids. 2010;58:1338–60.
32. Barbés B, Páramo R, Sobrón F, Blanco E, Casanova C. Thermal conductivity measurement of liquids by means of a microcalorimeter. J Therm Anal Calorim. 2010. doi:10.1007/s109730101169y.
33. Tian F, Sun L, Mojumdar SC, Venart JES, Prasad RC. Absolute measurement of thermal conductivity of poly (acrylic acid) by transient hot wire technique. J Therm Anal Calorim. 2011. doi: 10.1007/s1097301012613.
34. Maffezzoli A, Terzi R. Thermal analysis of visible light-activated dental composites. Thermochim Acta. 1995;269/270:319–35.
35. Micelli F, Maffezzoli A. Characterization of the kinetic behavior of resin modified Glass-ionomer cements by DSC, TMA and ultrasonic wave propagation. J Mater Sci Mater Med. 2001;12:151–6.
36. Farrar DF, Rose J. Rheological properties of PMMA bone cements during curing. Biomater. 2001;22:3005–13.
37. O'Brien DJ, Mather PT, White SR. Viscoelastic properties of an epoxy resin during cure. J Compos Mater. 2001;35:883–904.
38. Collyer AA, Clegg DW. Rheological measurement. New York: Elsevier Applied Science; 1988.
39. Kamal MR, Sourour S, Ryan M. Kinetic and thermal characterization of thermoset cure. Polym Eng Sci. 1973;13:59–64.
40. Sourour S, Kamal MR. Differential scanning calorimetry of epoxy-amine cure: isothermal cure kinetics. Thermochim Acta. 1976;14:41–59.

41. Kenny JM, Maffezzoli A, Nicolais L. A Model for the thermal and chemorheological behavior of thermoset processing: (II) unsaturated polyester based composites. Compos Sci Technol.1990; 38:339–58.
42. Maffezzoli A. Polymerisation kinetics of acrylic bone cements by differential scanning calorimetry. J Therm Anal. 1996;47:35–49.
43. Fournier J, Williams G, Duch C, Aldridge GA. Changes in molecular dynamics during bulk polymerization of an epoxide-amine system as studied by dielectric relaxation spectroscopy. Macromol. 1996;29:7079–107.
44. Haupt P. Continuum mechanics and theory of materials, 2nd edn. Berlin: Springer; 2002.
45. Holzapfel GA. Nonlinear solid mechanics: a continuum approach for engineering. Chichester: Wiley; 2000.
46. Böhme G. Strömungsmechanik nichtnewtonscher Fluide, 2nd edn. Stuttgart: Teubner Verlag; 2000.
47. Alberty RA. Use of legendre transforms in chemical thermodynamics. Pure Appl Chem. 2001;73(8):1349–80.
48. Höfer P. Dynamische Eigenschaften technischer Gummiwerkstoffe: experimente, thermomechanische materialmodellierung und implementierung in die FEM. München: Verlag Dr. Hut; 2009.
49. Haupt P, Lion A. On finite linear viscoelasticity of incompressible isotropic materials. Acta Mech. 2002;159:87–124.
50. Lion A, Kardelky C. The payne effect in finite viscoelasticity: constitutive modelling based on fractional derivatives and intrinsic time scales. Int J Plast. 2004;20:1313–45.